Transconductance Degradation in Near-THz InP Double-Heterojunction Bipolar Transistors

Vibhor Jain and Mark J. W. Rodwell, *Fellow, IEEE*

***Abstract*—We examine the relationship between transconductance g_m and emitter current density J_E for InP/InGaAs/InP abrupt emitter–base (EB) double-heterojunction bipolar transistors operating at high J_E. High J_E is needed to increase g_m for reduced C/g_m delays. We observe a significant degradation in measured g_m below qI_E/kT with increased J_E. This degradation primarily results from the Fermi–Dirac statistics governing current injection at high current densities and from quantum–mechanical reflection at the EB junction arising from changes in the electron effective mass and in the conduction band potential. Transconductance is further reduced by gradients in the quasi-Fermi level in the EB space-charge region and by modulation of the heterointerface energy barrier by the applied bias.**

***Index Terms*—Double-heterojunction bipolar transistor (DHBT), InGaAs, InP, scaling, transconductance.**

I. Introduction

TERAHERTZ (THz)-bandwidth double-heterojunction bipolar transistors (DHBTs) have potential application in 0.3- to 1.0-THz integrated circuits (ICs) for imaging, sensing, radio astronomy, and spectroscopy, in high-resolution 2- to 20-GHz mixed-signal ICs, and in 100- to 500-GHz digital logic [1]–[3]. Heterojunction bipolar transistor (HBT) bandwidth is increased by thinning the base and collector layers for reduced transit times, as well as by reducing junction widths and ohmic contact resistivities for reduced RC charging times. Because the collector–base capacitance per unit collector junction area, i.e., C_{cb}/A_c, increases as the collector depletion layer is thinned, the transconductance per unit emitter area g_m/A_e must increase in proportion to the square of transistor bandwidth to reduce C_{cb}/g_m charging time. At moderate applied base–emitter voltage V_{be}, electron density in the base and at the emitter–base (EB) heterojunction is nondegenerate; hence, current density $J_E \propto \exp(qV_{be}/NkT)$ exponentially varies with V_{be}, and the transconductance per unit emitter area $g_m/A_e = qJ_E/NkT$ is consequently proportional to J_E. J_E must therefore vary in proportion to the square of HBT bandwidth [3]–[5] to obtain the desired scaling of g_m.

InP/InGaAs DHBTs studied here have abrupt EB junctions. For these HBTs, g_m fails to increase in direct proportion to J_E at current densities greater than $\sim$2 mA/μm^2. The degradation in g_m increases the C_{cb}/g_m charging time and significantly degrades the bandwidth of HBTs having f_τ approaching or exceeding 500 GHz [6], [7].

Manuscript received April 27, 2011; accepted May 15, 2011. Date of publication June 20, 2011; date of current version July 27, 2011. This work was supported by the Defense Advanced Research Projects Agency THETA Program under Contract HR0011-09-C-0060. The review of this letter was arranged by Editor G. Meneghesso.

The authors are with the Department of Electrical and Computer Engineering, University of California, Santa Barbara, CA 93106 USA (e-mail: vibhor@ece.ucsb.edu; rodwell@ece.ucsb.edu).

Color versions of one or more of the figures in this letter are available online at http://ieeexplore.ieee.org.

Digital Object Identifier 10.1109/LED.2011.2157451

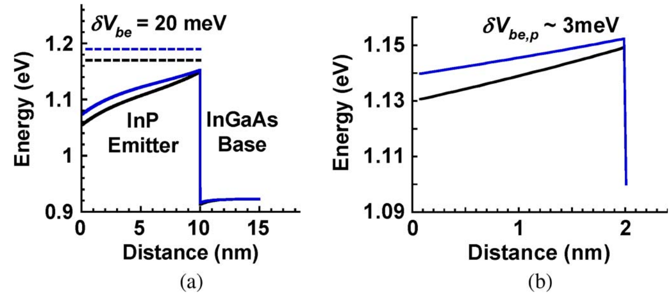

Fig. 1. (a) Band diagram from electrostatic simulation of the InP/InGaAs EB junction at two different applied V_{be} ($\delta V_{be} = 20$ meV). (b) Magnified E_c profile at the EB junction showing $\delta V_{be,p} = 3$ meV due to the barrier modulation effect; $\delta V_{\rm injection} = 17$ meV.

We here analyze significant contributors to g_m degradation in abrupt EB HBTs, including modulation of the EB electron injection barrier by applied bias V_{be}, drops in the electron quasi-Fermi level in the emitter space-charge region, and quantum–mechanical reflection and degenerate electron injection at the EB interface.

II. Barrier Modulation and Quasi-Fermi Level Drop

Given finite base doping N_A, applied V_{be} modulates the depletion region electrostatic potential on both the emitter and base sides of the barrier. Increasing V_{be} by δV_{be} in an HBT with an abrupt EB junction, the barrier for electron injection into the base is reduced by an amount $\delta V_{\rm injection} = \delta V_{be} - \delta V_{be,p}$, where $\delta V_{be,p}$ is the modulation of the electrostatic potential in the base (see Fig. 1). In contrast, in HBTs with graded EB junctions, $\delta V_{\rm injection} = \delta V_{be}$.

In addition, the electron flux has associated with it a drop

$$\Delta E_{fn} = \int\limits_{W_{\rm dep}} \frac{J_E}{\mu_n(x) \cdot n(x)} \cdot dx \qquad (1)$$

in the electron quasi-Fermi level [4] across the emitter space-charge region (see Fig. 2), where $W_{\rm dep}$ is the emitter space-charge region width, μ_n is the electron mobility, and $n(x)$ is the electron charge density. ΔE_{fn} increases with J_E for both graded and abrupt EB junctions. Writing $qV_{\rm injection} = E_{fn} - E_c$ at the EB junction, for an applied voltage δV_{be}, the barrier for electron injection is $\delta V_{\rm injection} = \delta V_{be} - \delta V_{be,p} -$

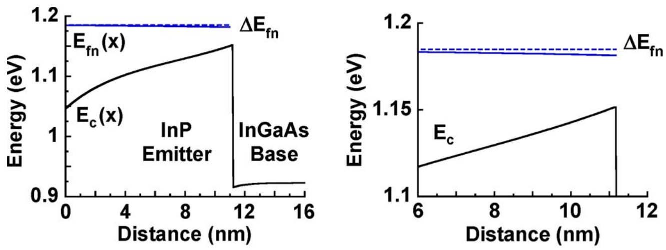

(a) (b)

Fig. 2. (a) Band diagram from electrostatic simulation of the InP/InGaAs EB junction. (b) Magnified E_c and E_{fn} profile at the EB junction showing a drop in quasi-Fermi level ΔE_{fn} in the emitter space-charge region at high J_E. $J_E \sim 20$ mA/μm^2 was used for this simulation.

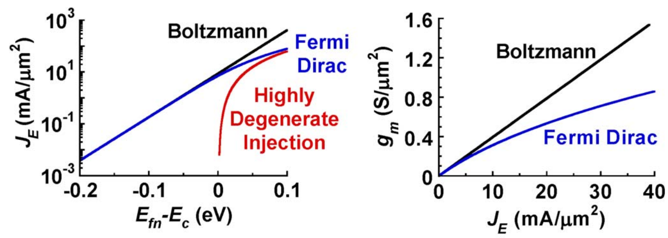

(a) (b)

Fig. 3. (a) Calculated J_E as a function of Fermi level E_{fn} position relative to conduction band edge E_c for the InP emitter for the Boltzmann approximation, Fermi–Dirac distribution function, and highly degenerate injection ($T = 0$ K or $q(V_{be} - \phi) \gg kT$). (b) Computed g_m as a function of J_E.

$\delta(\Delta E_{fn})/q$. Independent of the carrier statistics, the transconductance per unit emitter junction area is then reduced, i.e.,

$$\frac{g_m}{A_e} = \frac{\partial J_E}{\partial V_{be}} = \frac{\partial V_{\text{injection}}}{\partial V_{be}} \cdot \frac{\partial J_E}{\partial V_{\text{injection}}}$$
$$= \left(1 - \frac{\partial V_{be,p}}{\partial V_{be}} - \frac{1}{q}\frac{\partial(\Delta E_{fn})}{\partial V_{be}}\right) \cdot \frac{\partial J_E}{\partial V_{\text{injection}}}. \quad (2)$$

Given a 15-nm (W_{dep})-thick InP emitter doped at 2×10^{18} cm^{-3} capped above by 5×10^{19} cm^{-3} doped n$^+$ InP, and a p$^+$ InGaAs base doped at 9×10^{19} cm^{-3} [8], both $n(x)$ and $\partial V_{be,p}/\partial V_{be}$ are found by numerical simulation of the junction using a self-consistent Poisson/Fermi–Dirac algorithm [9]. J_E is then determined from E_{fn} at the InP/InGaAs interface using the methods described in Section III. ΔE_{fn} is finally computed from (1). At an applied V_{be} such that $J_E = 20$ mA/μm^2, we find $\partial V_{be,p}/\partial V_{be} = 0.17$, $\partial(\Delta E_{fn}/q)/\partial V_{be} = 0.05$, and $\partial V_{\text{injection}}/\partial V_{be} = 0.78$.

III. Degenerate Injection and Quantum–Mechanical Reflection

A. Degenerate Injection

At ~10–35 mA/μm^2 current densities necessary for 0.5- to 1-THz f_τ [3], electron Fermi level E_{fn} must approach conduction band energy E_c at the InP/InGaAs interface. The electron thermal statistics can then no longer be approximated by a Boltzmann distribution, and J_E no longer exponentially varies with E_{fn} [3]. Instead, the emitter current density is computed from the Fermi–Dirac distribution [3], [10], [11], i.e.,

$$J_E = \frac{qm^*}{2\pi^2\hbar^3}\int_0^\infty \frac{E}{1 + \exp\left((E - (E_{fn} - E_c))/k_B T\right)} dE \quad (3)$$

where q is the electron charge, m^* is the electron effective mass, k_B is the Boltzmann's constant, and $E_{fc} = E_{fn} - E_c$ is the Fermi level above the conduction band edge at the InP/InGaAs heterointerface. Equation (3) assumes a parabolic conduction band.

Fig. 3 compares J_E and g_m per unit junction area ($g_m/A_E = \partial J_E/\partial V_{be}$) for an InP emitter with $V_{be} = V_{\text{injection}}$ and for Fermi–Dirac and Boltzmann statistics at $T = 300$ K. At $J_E = 30$ mA/μm^2, degenerate electron statistics reduce g_m 1.7 : 1 relative to the nondegenerate case. Under degenerate injection, J_E no longer varies as $\exp(qV_{\text{injection}}/NkT)$, and g_m no longer varies as qI_E/NkT. Indeed, defining ϕ as the applied V_{be} at which $E_{fn} = E_c(x_{\text{barrier}})$, for highly degenerate injection such that $(V_{be} - \phi) \gg kT/q$ or for $T = 0$ K, $J_E = q^2 m^*(V_{be} - \phi)^2/4\pi^2\hbar^3$ [see Fig. 3(a)]; current varies in proportion to the square of applied V_{be}.

B. Quantum–Mechanical Reflection

Even given an electron Fermi level E_{fn} above conduction band barrier $E_c(x_{\text{barrier}})$, some fraction of the electron flux incident from the emitter is reflected at the InP/InGaAs interface [12]. This is a consequence of the abrupt change in both m^* and E_C. Ignoring the small additional electron wave reflection by the potential gradient within the InP emitter space-charge region, the electron transmission coefficient $T(E_{fc})$ at the InP/InGaAs interface is

$$T(E_{fc}) \cong \frac{4(m_1/m_2)^{1/2} E_{fc,x}^{1/2} E_t^{1/2}}{E_{fc,x} + (m_1/m_2)E_t + 2(m_1/m_2)^{1/2} E_{fc,x}^{1/2} E_t^{1/2}} \quad (4)$$

where $m_1 = 0.08 \cdot m_0$ is the effective electron mass in the InP emitter, $m_2 = 0.04 \cdot m_0$ is the effective mass in the InGaAs base, $E_t = E_b + E_{fc,x} + E_{fc,yz}(1 - m_1/m_2)$, E_b is the height of the barrier, and $E_{fc,x}$ and $E_{fc,yz}$ are the x and yz-components of the total electron kinetic energy above the barrier at the InP/InGaAs interface, respectively [see Fig. 4(a)]. The calculated $T(E_{fc})$ for $E_{fc,yz} = 0$ is shown in Fig. 4(b). J_E is now given by the following relationship [10]:

$$J_E = \iint 2q \cdot g(E_x, E_{yz}) \cdot f_{\text{FD}}(E_x, E_{yz}) \cdot v(E_x) \cdot T(E_x, E_{yz})\, dE_x\, dE_{yz} \quad (5)$$

where $g(E_x, E_{yz})$ is the density of states, $f_{\text{FD}}(E_x, E_{yz})$ is the Fermi–Dirac distribution function, and $v(E_x)$ is the electron velocity. Neglecting tunneling, we have assumed $T(E_x, E_{yz})$ to be zero for incident energy values below the barrier [10].

C. Correlation With Experimental Data

We now compare (see Fig. 5) the computed variation of g_m/A_E with J_E for all considered effects that degrade g_m. For clarity in presentation, the curves in Fig. 5 assume zero extrinsic emitter resistance R_{ex}, zero base access resistance R_{bb}, and infinite dc current gain β. At $J_E \sim 30$ mA/μm^2, there is more than a 2 : 1 reduction in g_m compared with the Boltzmann approximation. In [3] and [13], the deviation from Boltzmann statistics was modeled as a current-independent

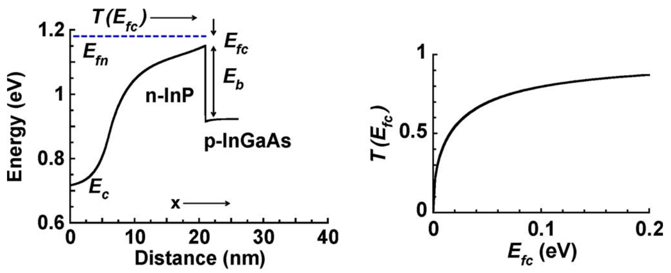

(a) (b)

Fig. 4. (a) Energy band diagram for computing transmission coefficient $T(E_{fc})$ over EB energy barrier E_b. (b) $T(E_{fc})$ as a function of energy E_{fc} above the barrier for $E_{fc,yz} = 0$ at the InP/InGaAs interface.

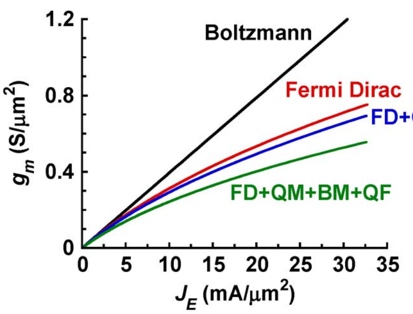

Fig. 5. g_m as a function of J_E at 300 K, including all possible effects causing g_m degradation. FD, Fermi–Dirac; QM, quantum–mechanical reflection; BM, barrier modulation effect; QF, quasi-Fermi level drop.

equivalent series resistance; this model fails to fit well the HBT characteristics for J_E exceeding 10 mA/μm^2.

Fig. 6 compares the variation of g_m/A_E with J_E computed from theory with that determined from bias-dependent 100-MHz to 2-GHz Y-parameter measurements using an Agilent E8361A network analyzer. The measured curves are for HBTs on the same wafer with $L_E = 3.5$ μm and $W_E = 120$, 180, 220 and 270 nm. The calculated g_m curves include $R_{\rm ex} = 3\ \Omega \cdot \mu{\rm m}^2$ and $R_{\rm bb}/\beta = 1\ \Omega \cdot \mu{\rm m}^2$. A curve for the Boltzmann approximation, including the effects of $R_{\rm ex}$ and $R_{\rm bb}/\beta$, has also been included in Fig. 6. Experimental values for $R_{\rm ex}$ are obtained from transmission-line method measurements of metal/InGaAs and InGaAs/InP interfaces on separate wafers, and $R_{\rm bb}$ is estimated from S-parameter and β from dc measurements. To include the effect of device self-heating, thermal resistance $R_{\rm th} = 5.1$ K/mW was calculated using the method in [14] for $V_{cb} = 0.7$ V. The device junction temperature rise calculated from $T_{\rm junc} = T_{\rm amb} + R_{\rm th} \cdot I_c \cdot V_{ce}$ at each J_E was then incorporated in (5) to compute J_E and g_m. The discrepancy at low J_E could result from neglecting tunneling through the barrier. It is to be noted from the data in Figs. 5 and 6 that measured g_m is dominated by extrinsic resistances.

IV. Conclusion

We have explored various effects degrading HBT g_m at high J_E. Barrier modulation and quasi-Fermi level drop due to the EB space-charge region can be reduced through increased doping in the emitter and base regions and through thinner emitter depletion layers. Quantum–mechanical reflection can be reduced by grading the EB heterojunction. To avoid g_m reduction from electron degeneracy, emitter semiconductors with increased density of states must be identified and employed.

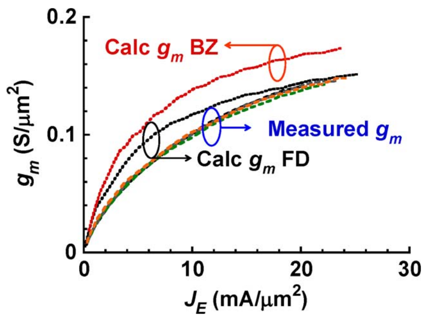

Fig. 6. Measured and calculated (FD, Fermi–Dirac; BZ, Boltzmann) g_m of different HBTs as a function of J_E, including the effects of $R_{\rm ex}$, $R_{\rm bb}$, β, and device self-heating. The calculated g_m FD curve also includes the effects in Fig. 5.

Acknowledgment

The authors would like to thank Prof. M. Lundstrom and G. Liang (Purdue University, West Lafayette, IN) for initial derivation of (3) for HBTs.

References

[1] J. Hacker, M. Seo, A. Young, Z. Griffith, M. Urteaga, T. Reed, and M. Rodwell, "THz MMICs based on InP HBT technology," in *Proc. IEEE MTT-S Int. Microw. Symp. Exhib.*, May 23–28, 2010, pp. 1126–1129.

[2] J. C. Zolper, "Challenges and opportunities for InP HBT mixed signal circuit technology," in *Proc. Int. Conf. Indium Phosphide Relat. Mater.*, May 12–16, 2003, pp. 8–11.

[3] M. J. W. Rodwell, M. Le, and B. Brar, "InP Bipolar ICs: Scaling roadmaps, frequency limits, manufacturable technologies," in *Proc. IEEE*, vol. 96, no. 2, pp. 271–286, Feb. 2008.

[4] M. J. W. Rodwell, M. Urteaga, T. Mathew, D. Scott, D. Mensa, Q. Lee, J. Guthrie, Y. Betser, S. C. Martin, R. P. Smith, S. Jaganathan, S. Krishnan, S. I. Long, R. Pullela, B. Agarwal, U. Bhattacharya, L. Samoska, and M. Dahlstorm, "Submicron scaling of HBTs," *IEEE Trans. Electron Devices*, vol. 48, no. 11, pp. 2606–2624, Nov. 2001.

[5] Z. Griffith, Y. Dong, D. Scott, Y. Wei, N. Parthasarathy, M. Dahlstrom, C. Kadow, V. Paidi, M. J. W. Rodwell, M. Urteaga, R. Pierson, P. Rowell, B. Brar, S. Lee, N. X. Nguyen, and C. Nguyen, "Transistor and circuit design for 100–200 GHz ICs," *IEEE J. Solid-State Circuits*, vol. 40, no. 10, pp. 2061–2069, Oct. 2005.

[6] Z. Griffith, E. Lind, M. J. W. Rodwell, X.-M. Fang, D. Loubychev, Y. Wu, J. M. Fastenau, and A. W. K. Liu, "60 nm collector InGaAs/InP Type-I DHBTs demonstrating 660 GHz f_T, $\mathrm{BV_{CEO}} = 2.5$ V, and $\mathrm{BV_{CBO}} = 2.7$ V," in *Proc. IEEE CSIC*, Nov. 12–15, 2006, pp. 275–278.

[7] W. Snodgrass, W. Hafez, N. Harff, and M. Feng, "Pseudomorphic InP/InGaAs heterojunction bipolar transistors (PHBTs) experimentally demonstrating $f_T = 765$ GHz at 25 °C increasing to $f_T = 845$ GHz at -55 °C," in *IEDM Tech. Dig.*, Dec. 2006, pp. 1–4.

[8] V. Jain, E. Lobisser, A. Baraskar, B. J. Thibeault, M. J. W. Rodwell, Z. Griffith, M. Urteaga, D. Loubychev, A. Snyder, Y. Wu, J. M. Fastenau, and W. K. Liu, "InGaAs/InP DHBTs in a dry-etched, refractory metal emitter process demonstrating simultaneous $f_t/f_{\max} \sim 430/800$ GHz," *IEEE Electron Device Lett.*, vol. 32, no. 1, pp. 24–26, Jan. 2011.

[9] W. Frensley, *Bandprof, Semiconductor Device Simulation Tool*, University of Texas, Dallas, TX.

[10] N. Machida, Y. Miyamoto, and K. Furuya, "Minimum emitter charging time for heterojunction bipolar transistors," in *Proc. Indium Phosphide Relat. Mater. Conf.*, 2006, pp. 325–328.

[11] C. Y. Chang and S. M. Sze, "Carrier transport across metal–semiconductor barriers," *Solid State Electron.*, vol. 13, no. 6, pp. 727–740, Jun. 1970.

[12] Q.-G. Zhu and H. Kroemer, "Interface connection rules for effective-mass wave functions at an abrupt heterojunction between two different semiconductors," *Phys. Rev. B, Condens. Matter*, vol. 27, no. 6, pp. 3519–3527, Mar. 1983.

[13] M. Yamada, T. Uesawa, Y. Miyamoto, and K. Furuya, "Deviation from proportional relationship between emitter charging time and inverse current of heterojunction bipolar transistors operating at high current density," *IEEE Electron Device Lett.*, vol. 32, no. 4, pp. 491–493, Apr. 2011.

[14] W. Liu, H.-F. Chau, and E. Beam, "Thermal properties and thermal instabilities of InP-based heterojunction bipolar transistors," *IEEE Trans. Electron Devices*, vol. 43, no. 3, pp. 388–395, Mar. 1996.